Journal of Hazardous Materials 189 (2011) 764–772

Contents lists available at ScienceDirect

Journal of Hazardous Materials

journal homepage: www.elsevier.com/locate/jhazmat

Sorption of selenium oxyanions on TiO_2 (rutile) studied by batch or column experiments and spectroscopic methods

Lenka Svecova[a,b,1], Manuel Dossot[b,*], Sébastien Cremel[c], Marie-Odile Simonnot[a], Michel Sardin[a], Bernard Humbert[b], Christophe Den Auwer[d], Laurent J. Michot[e]

[a] Laboratoire Réactions et Génie des Procédés, UPR CNRS n°3349, 1, rue Grandville BP 20451 54001 Nancy Cedex, France
[b] Laboratoire de Chimie Physique et Microbiologie pour l'Environnement, UMR 7564 CNRS-Nancy Université, 405, rue de Vandoeuvre, 54600 Villers-lès-Nancy, France
[c] Institut Pluridisciplinaire de Recherche sur l'Environnement et les Matériaux, UMR 5254 CNRS-Université de Pau, Hélioparc, 2 Avenue du Président Pierre Angot, 64000 Pau, France
[d] Commissariat à l'Energie Atomique de Valrho Marcoule, DCC/DRRV/SEMP, BP 171, 30207 Bagnols-sur-Ceze Cedex, France
[e] Laboratoire Environnement et Minéralurgie, UMR 7569 CNRS-Nancy Université, Pôle de l'Eau, 15 Avenue du Charmois, 54501 Vandoeuvre-lès-Nancy Cedex, France

ARTICLE INFO

Article history:
Received 9 September 2010
Received in revised form 25 February 2011
Accepted 28 February 2011
Available online 6 March 2011

Keywords:
TiO_2
Rutile
Selenites
Selenates
Sorption
Spectroscopy
Batch
Column

ABSTRACT

Selenium is a known toxic element released in the environment by anthropogenic activities. The present study is devoted to the aqueous sorption behaviour of selenium oxyanions (selenate and selenite) on a reference oxide surface, namely rutile TiO_2. Batch sorption kinetics and isotherms have been studied using different physico-chemical conditions of the solution (changes of pH and ionic strength). The sorption was favoured for both anions in acidic conditions, in agreement with a surface complexation mechanism and CD-MUSIC predictions. Spectroscopic investigations of the sorbed rutile powder were also consistent with such a mechanism. EXAFS spectra confirmed that for selenite anions, an inner-sphere mechanism was the most probable process observed. Dynamic sorption experiments using a column filled with rutile powder also substantiated that a part of the surface complexes follows the inner-sphere mechanism, but also evidenced that an outer-sphere mechanism cannot be excluded, especially for selenate anions.

1. Introduction

Though an essential trace element for health, selenium is toxic at moderate and high concentrations and can be bioaccumulated. Industrial and agricultural activities have contributed to increase the release of selenium species from geologic sources. Wild life in ecosystems can be strongly impacted by this release, coming from drain waters, sewage sludge, oil refineries or mining for instance [1]. Sporadic episodes of high concentration release have sometimes led to very harmful levels, with concentrations in drainage water approaching 140–1400 $\mu g\,L^{-1}$ [2]. To understand the mobility of selenium species in the environment and to propose remediation processes, it is of high importance to properly describe and understand the nature of the chemical bonds between solid materials (minerals of soils or specifically designed sorbent materials) and selenium species present in aqueous conditions. In natural aqueous environments, selenium can be found under two stable oxidation states: Se(IV), generally as a selenite oxyanion SeO_3^{2-} or in its protonated forms H_2SeO_3 and $HSeO_3^-$ ($pKa_1 = 2.64$ and $pKa_2 = 8.4$ [3]), and Se(VI) as a selenate oxyanion SeO_4^{2-}. Numerous studies have investigated the sorption of selenium oxyanions on various mineral surfaces such as iron oxy-hydroxides [4–14], aluminium oxy-hydroxides [15–20], hydrous titanium [21] or manganese [22] oxides, copper(I) oxides [23,24], cements and clays [3,25–29], soils or complex media [30–35], granite [36,37], hydroxyapatite [38], Mg/Fe carbonated layered double hydroxides [39] and iron sulphides [2,40]. In most of these sorption studies [3–40], Se(IV) appeared to be more retained by the solid surface than Se(VI). Sorption on oxy-hydroxide compounds was found to be pH-dependent, thus suggesting a surface complexation mechanism. In the case of iron or aluminium oxy-hydroxides, the molecular structure of the surface complexes formed remains highly debated [4–20,41]. For instance, EXAFS spectroscopy was performed to study the sorption of selenate and selenite ions on goethite α-FeO(OH)[13,14]. It was found that selenite ions were sorbed as inner-sphere complexes (through the formation of a covalent Fe–O–Se bond), whereas selenate ions were sorbed as

* Corresponding author. Tel.: +33 3 83 68 52 49.
E-mail address: manuel.dossot@lcpme.cnrs-nancy.fr (M. Dossot).
[1] Current address: Laboratoire d'Electrochimie et de Physicochimie des Matériaux et des Interfaces, UMR 5631 CNRS-INPG-UJF, 1130 rue de la piscine, 38402 Saint-Martin d'Hères Cedex, France.

0304-3894/$ – see front matter © 2011 Elsevier B.V. All rights reserved.
doi:10.1016/j.jhazmat.2011.02.090

outer-sphere complexes having a hydration shell around sorbed selenium oxyanions. However, Su and Suarez [10] reported infrared absorption spectra that were in better agreement with inner-sphere complexes for the sorption of both Se(IV) and Se(VI) species on goethite and amorphous iron oxide. The main difficulty in most of the previous studies relies on the fact that the surface hydroxyl groups of the sorbent materials were not totally characterized or were widely distributed among several structural sites. Studies of the sorption of selenium species on well characterized surface is thus of high importance to depict the nature and molecular structure of surface complexes. Once having such information, it will be possible to discuss the role of the molecular structure of selenite and selenate on their sorption properties. Why either the inner-sphere or outer-sphere complex is formed is not straightforward but appears to depend on many parameters:

(i) The morphology of the sorbing material [17], i.e. its specific surface area, the various crystallographic faces that are expressed, and the accessibility of the solution to the surface sites. This morphology might be more favourable towards selenite or selenate species, in relation to their molecular structure.
(ii) The physico-chemical parameters of the solution (pH, ionic strength, composition of the background electrolyte) that can influence the speciation of the selenium oxyanions both in solution or at the solid surface [17,41].
(iii) The sampling conditions used to perform the analysis, especially the difference between in situ experiments (keeping the solution/solid interface) or *ex situ* techniques that may involve air or vacuum drying [12] leading to a possible reorganisation of the surface complexes. It therefore appears that despite all these sorption studies, numerous questions remain open about the structure of the surface complexes of selenium. Some of the difficulties are sometimes linked to the solid surfaces investigated that can be either stable in a narrow pH range only, or difficultly modelled by *ab initio* calculations due to their complicated surface chemistry. For these reasons, analyzing the interaction of selenium oxyanions with rutile surfaces could represent a very fruitful approach. Indeed, though scarce in natural environments, rutile presents numerous advantages for a fundamental study. (i) It can be used in both powder and single crystal forms [42,43], which allows studying the possible influence of surface termination on reactivity; (ii) it is stable over a wide pH range (from pH 2 to 10 [42,44]); (iii) its surface science has been widely investigated and the knowledge of the surface hydroxyl groups is well documented [42,45]; (iv) finally, experimental results can be compared to *ab initio* calculations thorough DFT modelling of TiO_2 surfaces as has recently been carried out [46–49]. Two recent studies have dealt with the sorption of selenium oxyanions on TiO_2, mainly in the anatase phase [50,51], but to our knowledge, a complete study devoted to a well characterized rutile phase [52] has not yet been performed. The objective of the present paper is thus to study the sorption on the rutile surface of two oxyanions of selenium (selenite SeO_3^{2-} and its hydrogenated forms; selenate SeO_4^{2-}) both in batch and column at dynamic conditions. In our controlled conditions, no redox interchange has been observed between these two oxidation states of selenium. The column experiments have been performed to obtain information under hydrodynamic conditions that are closer to the situation encountered in natural environments. They offer the opportunity to check the sorption kinetics out of thermodynamic equilibrium and enable to study the competition with other anions. These column experiments are also performed in a shorter period of time if compared to batch conditions, and this can avoid side-effects such as solid dissolution. Comparison between batch and column experiments is thus always valuable.

2. Materials and methods

2.1. Materials

Titanium dioxide was purchased from CERAC Inc. (Milwaukee, USA). It is a very fine powder of the rutile allotropic form. Before use, the powder was extensively rinsed with deionised water. To remove possible surface contaminants, the powder was then washed for 30 min in 0.1 mol L^{-1} KOH. After thorough rinsing with MilliQ water the powder was then washed for 30 min in 0.1 mol L^{-1} HNO_3. The material was finally washed with MilliQ water until the rinsing liquid exhibited a constant pH and conductivity. The physicochemical parameters of this rutile powder have been reported in detail in our previous article [52]: e.g. specific surface area 5 m^2 g^{-1}, diameters of particle aggregates mainly distributed between 200 nm and 1 μm, and pH value of the point of zero charge (pH_{PZC}) ~ 4.5–5.

2.2. Sorption experiments

Sorption experiments were performed both in batch and dynamic systems. Batch sorption tests were carried out using the original powder, whereas, as previously explained [52], dynamic experiments were performed in a fixed bed column filled with compacted rutile powder. This compacted material was shown to possess the same physico-chemical parameters as the initial powder [52]. Batch sorption tests were performed first in order to determine the optimum parameters to be used in dynamic (column) sorption experiments.

Batch sorption experiments included the determination of sorption kinetics and sorption isotherms with a detailed investigation of the influence of both pH and ionic strength on retention capacity. Each experiment was performed following a two-step procedure that is described in detail in the supporting material. The first one was a hydration phase at given pH and ionic strength imposed by sodium perchlorate (see supporting information). This served to reach equilibrium condition for protonation/deprotonantion of surface hydroxyl groups of rutile vs. pH of the solution. For this step, 0.2 g of rutile powder was contacted with 10 mL of solution. Selenium sorption was then performed in a second step. Sorption isotherms were measured at pH 3 with initial concentrations in selenium oxyanions ranging between 5×10^{-5} and 5×10^{-3} mol L^{-1} (between ca. 6 and 600 ppm for selenite, and 7 and 700 ppm for selenate). Sorption time was fixed at 100 h. The selenium retention capacity was then calculated according to the mass balance equation (Eq. (1)):

$$q = \frac{V}{m}(C_0 - C_f) \quad (1)$$

where q is the retention capacity [μmol g^{-1}], V the volume of solution [mL], m the sorbent sample mass [g], and C_0 and C_f are the initial and final selenium concentration [μmol mL^{-1}] in the solution, respectively. The total selenium concentration in solution was determined using inductively coupled plasma atomic emission spectroscopy (ICP-AES) after filtration of the supernatant through a 0.22 μm filter. The speciation in solution was determined by ionic chromatography as for column experiments (see below) for several batch experiments to verify that no change of speciation occurred due to any oxido-reduction process. Experimental details are reported in the supporting information. For investigating the effect of pH and ionic strength, batch selenium sorption experiments were also carried out according to a protocol similar to that used in sorption kinetics measurements with hydration and sorp-

tion sequences lasting 12 and 100 h, respectively. The influence of solution pH (ranging between pH 2 and 12) was investigated under three ionic strength conditions (no background electrolyte, $[NaClO_4] = 10^{-3}$ and 10^{-1} mol L^{-1}) at constant concentration in selenium oxyanions (10^{-3} mol L^{-1}) and after 100 h. Column experiments were performed using the following experimental layout. A thermo-regulated OMNIFIT glass column (inner diameter 1 cm, height 10 cm) was filled with TiO_2 granules (prepared by compacting the 112–200 μm size fraction of TiO_2 powder according to reference [52]). The column was connected to an HLPC pump (Altech) and the solution was pumped in the up-flow direction. The system was further equipped with online pH (Ingold 611 pH probe from Mettler Toledo and PHM 210 pH meter from Tacussel) and conductivity probes (conductimeter from Pharmacia), a thermo-regulated bath (Polystat CC3 from Huber) and a fraction collector (Gilson 206). Prior to their introduction into the system, the solutions were out gassed by nitrogen bubbling. It should be noted here that the results obtained by batch and column experiments were very close (see below), which means that carbonate species that may be present in batch solution do not influence significantly the selenium sorption on TiO_2.

The column was filled with 7.88 g TiO_2 granules [52]. The total volume was 5.5 mL. On the basis of separately performed residence time distribution experiments using NaCl and $NaClO_4$ solutions, the porous volume of the fixed bed of the column was determined at a value of 3.5 mL. Consequently, the column bed has a high total porosity of 63.5%, which is appropriate for carrying out dynamic experiments.

The system was first conditioned at pH 3 with a 0.1 mol L^{-1} sodium perchlorate solution. This solution was pumped into the system till the effluent pH was stable and equal to its inlet value. Using such conditions, positively charged sorption sites are formed. This pH value was selected as the optimum pH on the basis of batch sorption results. The selenium inlet concentration was fixed at 0.001 mol L^{-1} with a background ionic strength of 0.1 mol L^{-1} of $NaClO_4$. The flow rate was fixed at 0.2 mL min^{-1}. The effluent pH and conductivity were recorded by online acquisition and the effluent samples were collected and analyzed using ionic chromatography (ICS 3000 device by Dionex) in order to analyze selenium speciation at the column outlet. Ionic chromatography enabled to clearly separate these two anions since the retention time of selenite and selenate anions were different. More details are given in the supporting material section.

Desorption experiments were also carried out under two different experimental conditions. Alkaline desorption was tested first using a 0.1 mol L^{-1} $NaClO_4$ solution at pH 11 pumped to the system at 0.2 mL min^{-1} immediately after the breakthrough. An acidic desorption procedure was also implemented. In this procedure, the saturated column was first fed with 0.1 mol L^{-1} $NaClO_4$ at pH 3 at the same flow rate, before carrying out an alkaline desorption. The desorbed amounts of selenium anions were then calculated and compared. The column was finally regenerated by acid conditioning, as described above.

2.3. Spectroscopic analyses

Raman spectra were recorded using a Jobin-Yvon T64000 spectrometer with a multi-channel CCD detector cooled with liquid nitrogen. The Raman scattering signal was collected at 180° via a confocal microscope equipped with a 100× objective (numerical aperture NA = 0.95). The theoretical lateral spatial resolution was ca. 0.25 μm and the theoretical axial spatial resolution was ca. 0.8 μm. The excitation source was an He:Ne laser operating at 633 nm (3 mW were focused on the sample) and the Rayleigh scattering was blocked using a Notch filter.

XPS analyses were carried out with a Kratos Axis Ultra (Kratos Analytical, UK) spectrometer with a hemispherical energy analyser using a monochromatic Al Kα source (1486.6 eV). As the delay-line detector provides a high count rate, the power applied to the X-ray anode was reduced to 90 W, thus minimizing any possible X-ray induced degradation of the sample. The instrument work function was calibrated to give a binding energy (BE) of 83.96 eV for the Au $4f_{7/2}$ line for metallic gold while the spectrometer dispersion was adjusted to give a BE of 932.62 eV for Cu $2p_{3/2}$ line for metallic copper. The samples were attached to the sample holder and pumped overnight prior to analyses. The pressure in the analysis chamber during XPS analysis was in the low 10^{-9} mbar range. All spectra were recorded at a 90° take-off angle, the analyzed area being routinely a spot ca. 700 μm wide but when necessary the analyzed area was reduced to a spot approximately 27 μm wide. Survey spectra were recorded with a 1.0 eV step and a 160 eV analyser pass energy. High resolution regions were analyzed with a 0.05 eV step and a 20 eV pass energy (instrumental resolution better than 0.5 eV). In both cases, the hybrid lens mode was employed. The spectra were analyzed using the Vision software from Kratos (Vision 2.2.0). A Shirley baseline was used for background subtraction.

EXAFS experiments were performed on the SAMBA beamline at the SOLEIL synchrotron facilities in France. The analysis was done at the K edge of Se at ~12.7 keV. Energy drift was corrected using standard Se_0 samples. The transmission experiments used the ionization chamber as detector. Si(1 1 1) crystals were used as monochromators providing an energy resolution $\Delta E/E = 1.2 \times 10^{-4}$ at 5 keV. The spot size of the beam on the sample was 200 μm × 300 μm. More information on the beamline technical data is available at: http://www.synchrotron-soleil.fr/Recherche/LignesLumiere/SAMBA.

The aqueous selenite solution for reference EXAFS spectrum was measured using $[Na_2SeO_3] = 0.05$ mol L^{-1}, natural pH 6 and no sodium perchlorate.

3. Results and discussion

3.1. Sorption kinetics and isotherms

The sorption kinetics obtained from ICP-AES analysis of the solutions for selenite and selenate species on rutile powder for two different acidic pH values are plotted in Fig. 1. Since the pH_{PZC} value of the rutile powder used in the present study is between 4.5 and 5 [52], sorption kinetics were accordingly studied at pH 3 and 5. Negligible (less than 0.2 units) pH changes were observed upon sorption. For both selenium oxyanions, the retention capacity reached 90% of its maximum value at the end of the first hour. The sorption kinetics of Se(IV) anions on the anatase form of TiO_2 was also reported to be a fast process at pH 3 [51]. Duc et al. [7] reported a 90% removal of selenite anions within the first 5 min upon sorption on haematite (haematite 16 g L^{-1}, 4×10^{-4} mol Se L^{-1}, 0.1 mol L^{-1} of $NaNO_3$ as background electrolyte) at pH 3.5, whereas much slower kinetics were observed at pH 7. A similar trend was observed in our case with a clear decrease in the removal rate of selenate and a slight decrease in the removal rate of selenite when the pH increased from 3 to 5. In Refs. [50,51], the decrease of the sorption efficiency with the increase of pH was reported for the sorption of selenite and selenate anions on TiO_2 anatase. In another study, Duc et al. [9] compared the kinetics of selenite and selenate sorption on goethite, magnetite and apatites (hydroxyapatite, fluoroapatite). Interestingly, the equilibrium was reached within minutes in the cases of iron oxides, for which a surface complexation mechanism was proposed, while 10 days were necessary in the case of apatite in agreement with an ion exchange process. The rapid sorption step observed in the present study could therefore suggests

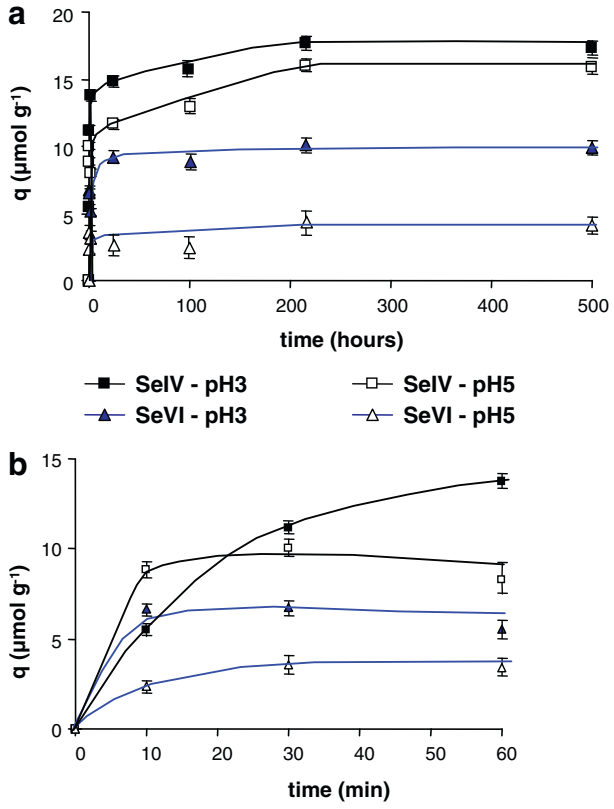

Fig. 1. (a) Comparison of selenite and selenate sorption kinetics (pH 5 and 3, 20 g TiO_2 L^{-1}, 0.001 mol Se L^{-1}, 0.01 mol L^{-1} $NaClO_4$); (b) detail of the first hour of experiment. Lines are only visual guides to indicate the kinetic trends.

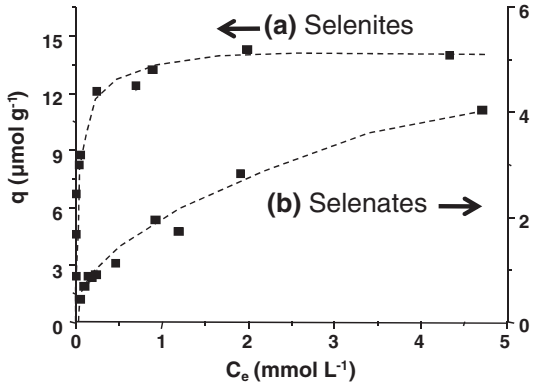

Fig. 2. Comparison of selenite and selenate sorption isotherms (pH 3, 20 g TiO_2 L^{-1}, contact time 100 h, $[NaClO_4] = 10^{-2}$ mol L^{-1}). Dashed lines are only visual guides.

the presence of surface complexation mechanisms, as reported for anatase sorbent material [50,51]. Following this rapid initial step, a slower increase is observed for selenite anions, with a plateau value reached between 100 and 200 h. Raman experiments have shown that perchlorate anions can be partly sorbed at the rutile surface (see below), most probably as outer sphere surface complexes. At long contact times, the selenite anions might partly compete with these perchlorate anions if thermodynamics is favourable, resulting in a sorption as outer-sphere complexes and an increase of the retention capacity.

Fig. 1 clearly reveals that for the same contact time and pH, the sorption of selenite species was higher than the sorption of selenate species, by a factor ~2–4. Furthermore, the retention capacity as deduced from the plateau value in Fig. 1a diminished when pH increased from 3 to 5. In view of the pH_{PZC} value of the rutile powder, such an observation agrees with results previously reported for other oxide materials [4–24] showing that anion sorption is favoured if the surface of the solid material is positively charged. Using sorption kinetics results displayed in Fig. 1, the most appropriate contact time to study sorption isotherms was chosen at 100 h. Using such a time, the possible exchange effect observed at longer contact times with selenite anions was avoided while maintaining retention capacity higher than 95%. Fig. 2 reports the sorption isotherms obtained at pH 3 from ICP-AES analysis of the solutions for selenite and selenate species using $[NaClO_4] = 10^{-2}$ mol L^{-1} as background electrolyte. We here define q as the amount of adsorbed metal per unit weight of sorbent [µmol g^{-1}], q_m the maximum retention capacity under the given experimental conditions [µmol g^{-1}] and C_e the remaining (or equilibrium) ion concentration in solution [mmol L^{-1}]. The sorption isotherms for selenite and selenate anions were clearly different. The selenite sorption isotherm displayed a sharp increase of q at low C_e values, before q levelled off and reached a plateau value. The selenate sorption isotherm displayed a different shape and no true plateau was ever reached even at $C_e = 5$ mmol L^{-1}. Both isotherms were fitted using Langmuir and Freundlich equations (see Supporting Information, Figure S2 and Table S2). It must be pointed out that both these models were developed at the solid–gas interface and are in principle not applicable to the mineral–solution interface. Still, they are commonly used to investigate solid–solution interfaces as they provide estimates of the maximum retention capacity q_m. The models, equations and results are summarized in the supporting information section. The results showed that q_m was 2–4 times higher for selenite ($q_m \sim 13$ µmol g^{-1}) compared to selenate ($q_m < 4$ µmol g^{-1}) anions, which concurred with the results reported in Fig. 1. A decrease of retention capacity for selenate anions compared to selenite anions was reported for sorption on anatase TiO_2 [50], which indicates that the rutile and anatase phases, despite their change of crystallographic structure, behave similarly towards selenium oxyanions.

3.2. Effect of pH and ionic strength

Fig. 3a and b presents the influence of pH on the retention of selenite and selenate, respectively for three ionic strengths: no background electrolyte, $[NaClO_4] = 0.001$ and 0.1 mol L^{-1}. The retention rates of selenite and selenate were determined by analyzing the residual concentration of selenium in solutions by ICP-AES. Selenite retention progressively decreased with increasing solution pH (Fig. 3a) and above pH 8, nearly no selenite anions were sorbed onto rutile. Selenite speciation (speciation modelling performed with MEDUSA software [53]) shown in Fig. 3c allowed correlating the retention capacity with the aqueous Se(IV) speciation. The global trend was that acidic forms of selenite (H_2SeO_3 or $HSeO_3^-$) appeared to be more retained by the rutile powder than SeO_3^{2-}. However, this conclusion should be balanced by the fact that when the solution pH increased, hydroxyl groups at the rutile surface deprotonated. Two kinds of surface oxygen atoms are present at the rutile surface: "bridging oxygen" atoms shared by two Ti atoms and "terminal oxygen" atoms only bonded to one Ti atom. pKa values corresponding to these two sites were calculated by the bond valence model using the CD-MUSIC approach, which yielded values of pKa_1 (Ti_2OH/Ti_2O^-) = 4.36 and pKa_2 ($TiOH_2^+/TiOH$) = 7.52 [46–49]. Other values have been obtained in the literature on the basis of fitting results of a surface charge complexation model to experimental titration data. For instance, Machelevski et al. reported pKa_1 (Ti_2OH/Ti_2O^-) = 4.9 and pKa_2 ($TiOH_2^+/TiOH$) = 5.95 [54,55]. The difference between the two approaches lies mainly in the value of pKa_2. In the framework of the present study, these differences only marginally affected the

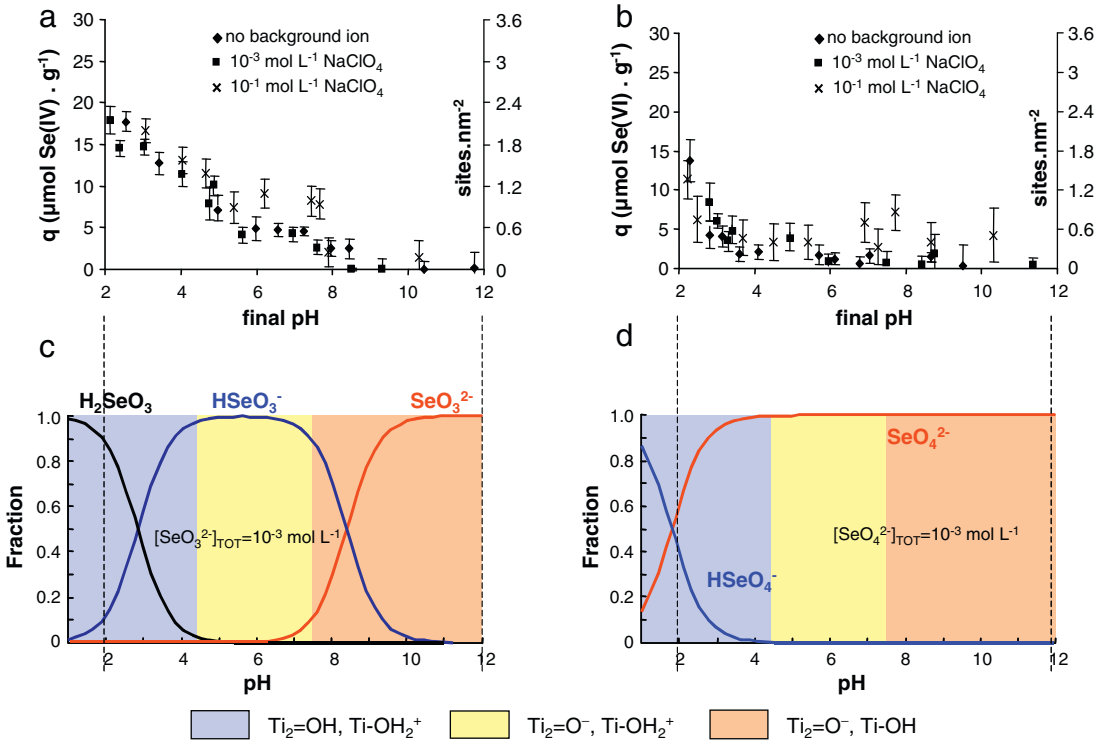

Fig. 3. (a and b) Influence of pH and ionic strength on selenite and selenate retention (contact time – 100 h, 0.001 mol Se L^{-1}, 20 g TiO_2 L^{-1}); (c and d) speciation modelling performed with Medusa program [51]. The main contributing surface hydroxyl groups of TiO_2 are also indicated, based on the following p*K*a values: pKa_1 (Ti_2 = OH/Ti_2 = O^-) = 4.36, pKa_2 ($TiOH_2^+$/TiOH) = 7.52 (see text).

results since most sorption experiments, either in batch or in column, were carried out at an acidic pH (below 5). The predominance of the different surface species based on the calculated p*K*a values are displayed in Fig. 3c as coloured regions. According to these results, the sorption of more than one selenite form might be considered, as reported in the case of selenite sorption on goethite [49]. In that latter case, two different inner-sphere complexes, X-$HSeO_3$ and X-SeO_3^- were evidenced. A similar type of situation could be deduced from the results in Fig. 3a. In the case of selenate sorption (Fig. 3b), a drastic loss in retention capacity was observed with increasing pH, leading to a so-called sorption edge. Above pH 5, as already observed in Fig. 1, nearly no selenate anions were retained at the rutile surface. Similar calculations (Fig. 3d) as those presented for selenite sorption strongly suggested that the adsorbed species was $HSeO_4^-$. Indeed, below pH 3 the retention capacity was higher while the rutile hydroxylation state did not change significantly. Similar trends were already reported in the case of selenate adsorption on magnetite [8] as well as on Fe hydroxide (at pH 6) and goethite at pH 4–5 [10].

3.3. Spectroscopic analyses

XPS, Raman and EXAFS spectroscopies were applied on dried powders in order to identify and quantify the selenium species sorbed at the rutile surface.

3.3.1. XPS and Raman

The detailed results of XPS experiments are given in Section 4 of the supporting material. The XPS spectra enabled determining the oxidation state of the selenium species sorbed at the surface of TiO_2 powder. It confirmed that no change of oxidation state occurred if compared to the sorbing solution. The amount of each selenium species detected at the surface of TiO_2 vs. pH of the solution for selenate and selenite species is given in Tables S4 and S5 of supporting material and are summarized in Fig. 4. This figure clearly confirmed the information deduced from solution analyses of residual selenium concentrations by ICP-AES (Figs. 1–3). For both anions, the amount of sorbed selenium was higher at low pH values. Se(IV) was better retained than Se(VI). Se(VI) signals beyond pH 3 were

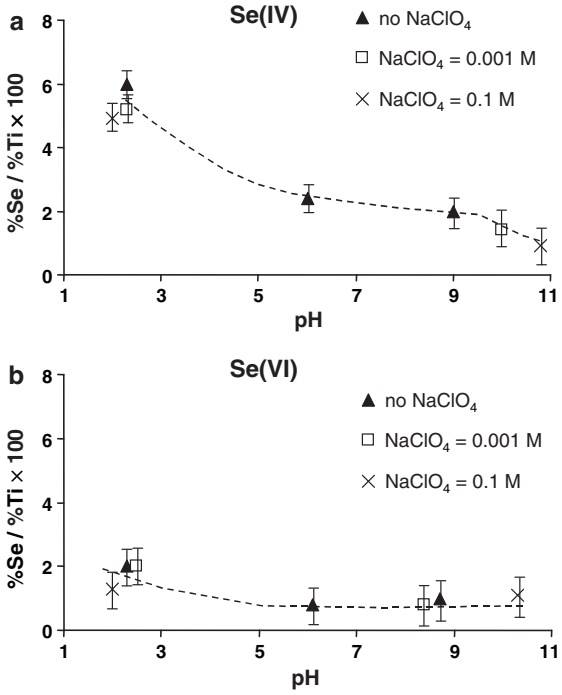

Fig. 4. Influence of pH and ionic strength on the selenite and selenate amount (normalized by the amount of Ti atoms) obtained at the surface of the TiO_2 powder by XPS analysis (contact time – 100 h, 0.001 mol Se L^{-1}, 20 g TiO_2 L^{-1}).

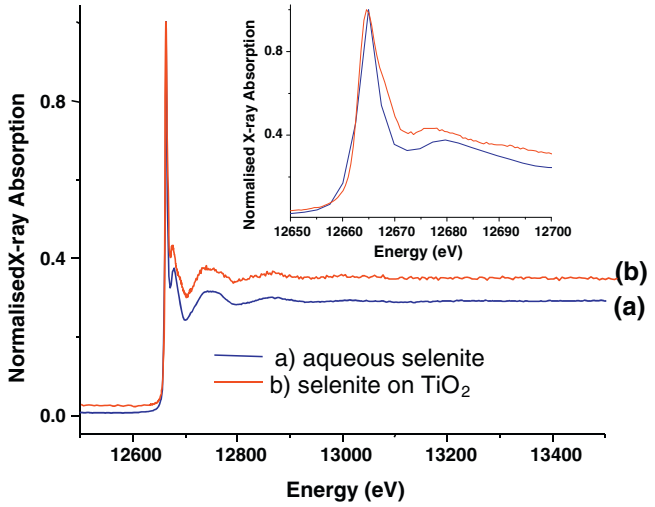

Fig. 5. Normalized X-ray absorption spectra for (a) an aqueous solution of selenite at pH 6 and (b) for the rutile powder with sorbed selenite species (solution conditions: $[Se(IV)] = 5 \times 10^{-2}$ mol L^{-1}, $[NaClO_4] = 0.01$ mol L^{-1}, pH 3). Insert compares the XANES spectra.

very low (some orders of magnitude below the detection limit), which corresponded to the sorption edge reported in Fig. 3b. In the case of selenite sorption, XPS analyses revealed two features that should be pointed out: (i) very low amounts of Se atoms were still detected at pH 10 and (ii) the sorption on the powder at pH 2 was only twice the value at pH 5. This contrasts with sorption results (Fig. 3a) where the amount of sorbed selenium at pH 2 was more than 4 times the value at pH 5. Point (i) could be explained by the high surface sensitivity of XPS compared to ICP-AES measurements of the solution. Point (ii) could be explained either by a reorganisation of the surface complexes at the surface of the rutile powder under vacuum in the XPS chamber (drying effect) or by a leaching of the possibly formed outer-sphere surface complexes occurring upon rinsing of the powder by distilled water prior to XPS analysis. XPS and Raman studies also show that perchlorate anions adsorbed at the rutile surface for ionic strengths as low as 2×10^{-3} mol L^{-1}.

3.3.2. EXAFS

Information about the outer or inner-sphere nature of the surface complexes could be obtained from EXAFS experiments at the Se K-edge. In view of the very limited amount of sorbed selenate anions, the only rutile powders analyzed were those obtained after selenite adsorption. Fig. 5 displays normalized X-ray absorption spectra obtained for a reference solution of aqueous selenite (pH 6, $[Se(IV)] = 10^{-2}$ mol L^{-1}), and for a TiO_2 powder after selenite adsorption ($[Se(IV)] = 5 \times 10^{-2}$ mol L^{-1}; $[NaClO_4] = 0.01$ mol L^{-1}, pH 3). Fig. 6 plots the extracted k^2-weighted EXAFS function $k^2\chi(k)$ vs. k, and the corresponding fits of the data using the model and parameters compiled in Table 1. For aqueous selenite anions, the experimental data could be satisfactorily reproduced using a first shell of three O atoms at 1.70 Å. At pH 6, according to the speciation of selenite anions (Fig. 3c), the main species present should be $HSeO_3^-$. One may then expect one Se–O bond length to be slightly different from the two other ones due to the protonation of one O atom. However, slightly changing one Se–O bond distance did not improve the fit significantly in view of the signal-to-noise ratio of the spectrum, and it was thus not possible to confirm its occurrence univocally. The fit of the EXAFS spectrum of selenite sorbed on TiO_2, revealed similar Se–O distances as in solution. An additional second shell contribution interpreted as due to two Ti atoms at 3.43 Å was also needed to fit the data. This contribution was clearly seen in the pseudo radial distribution function displayed in the right part of Fig. 6b. The appearance of such a Se–Ti distance was compatible with the formation of an inner-sphere surface complex. EXAFS experiments then clearly indicated the occurrence of surface complexation to form an inner-sphere complex in agreement with adsorption isotherm results.

Table 1
Main parameters used for the fits of EXAFS spectra (S_0^2 passive electron reduction factor (a.u.), e_0 energy shift in eV, r correlation coefficient in %).

Sample	First shell atoms		Parameters
Se(IV) aquo	3O at 1.70(1) Å $\sigma^2 = 0.0001$ Å^2	n.a.	$S_0^2 = 0.69$; $e_0 = 6.18$; $r = 5.4\%$
Se(IV)/TiO_2 powder	3O at 1.69(1) Å $\sigma^2 = 0.0009$ Å^2	2Ti at 3.43(8) Å $\sigma^2 = 0.0097$ Å^2	$S_0^2 = 0.76$; $e_0 = 1.05$; $r = 4.8\%$

3.4. Selenium sorption/desorption study in column experiments

On the basis of the results of batch experiments, dynamic sorption in a bed column packed with compacted rutile was performed at pH 3 and low selenium concentrations ($\leq 10^{-3}$ mol L^{-1}). All column experiments were performed at constant ionic strength (0.1 or 0.05 mol L^{-1} of $NaClO_4$). Prior to the sorption, the system was conditioned at pH 3. In order to ensure sufficient contact time, a low flow rate was selected, namely 0.2 mL min^{-1}. The effluent samples were collected regularly and analyzed later, while online acquisition of effluent pH and conductivity allowed an on-line monitoring of the experiments.

To properly monitor the selenate breakthrough curve, the selenate inlet concentration was fixed at 5×10^{-4} mol L^{-1} due to the rapid breakthrough of this anion. Fig. 7a displays the corresponding breakthrough curve thus obtained as well as the evolution of the normalized conductivity noted c/c_0 and pH of the effluent vs. V/V_p. The normalized conductivity was calculated according to Eq. (2):

$$\frac{c}{c_0} = \frac{c - c_{min}}{c_{max} - c_{min}} \quad (2)$$

In Eq. (2), c is the actual conductivity value, c_{min} is the minimum of conductivity obtained during the experiment, and c_{max} the maximum conductivity value.

A sharp increase in conductivity at low V/V_p was followed by a slight decrease and finally a return to the maximum value ($c/c_0 = 1$). The sharp initial increase of conductivity was due to the breakthrough of the electrolyte anions, whereas the other changes are mainly related to modifications of the effluent pH (variation of ca. 0.9 pH unit). Due to high molar conductivity and mobility of H^+ ions, their presence strongly increased the solution conductivity. These changes were more or less concomitant with selenate breakthrough. The highest pH value was recorded soon after the breakthrough value of V/V_p. As the saturation of the column continued, a progressive pH decrease was observed (above $V/V_p = 7$). The effluent pH was stabilised at the inlet value when the column was saturated. pH changes during the experiment could indicate that a retention mechanism through an inner-sphere complexation that involves proton consumption during the sorption process.

Selenite sorption reveals similar features (Fig. 7b, realized with an inlet concentration of 10^{-3} mol L^{-1} of selenite) with, however, a lower pH increase (+0.4 pH unit) and a delayed breakthrough moment (5 times later), compared to selenate. This latter difference revealed that the retention capacity of the column was 5 times higher with selenite anions than with selenate anions, which concurred with all the above discussed batch results. The total quantity of adsorbed selenium (q_{total}) was calculated by integrating the area below the breakthrough curve. The equilibrium retention capacity (q_{eq}) was then obtained by dividing this value by the mass of solid in the column. The results reported in Table 2 show retention

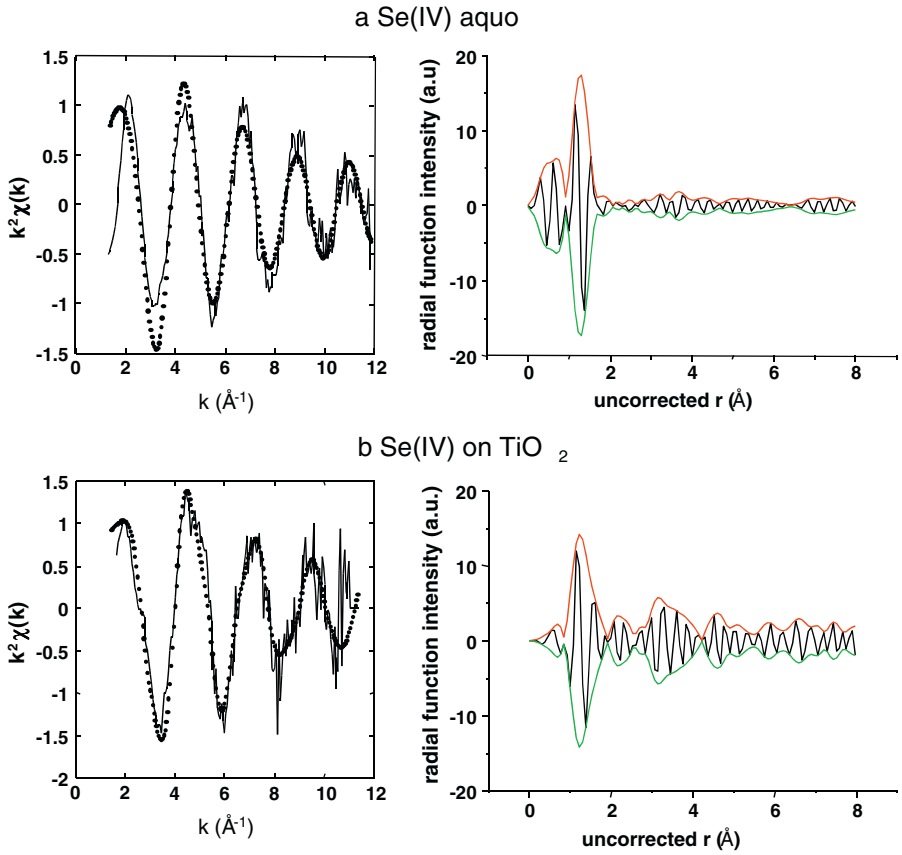

Fig. 6. k^2-Weighted EXAF spectra of Fig. 5 in k-space, fits of these spectra based on the parameters reported in Table 1, and corresponding pseudo radial distribution functions.

capacities of ca. 2–3 μmol g^{-1} for selenate and ~15 μmol g^{-1} for selenite. These values are in very good agreement with both the maximum value q_m estimated from Fig. 2 and the Langmuir and Freundlich fits reported in the supporting material (section 3). It thus appeared that rutile behaved in the same way whether powdered or compacted form. It also confirmed that, in hydrodynamic conditions, selenium oxyanions had access to all the sorption sites inside the rutile grains forming the column bed.

Once the sorption cycle was completed, the alkaline desorption cycle was studied and the results are given in the supporting material (Figure S5). The column saturated with selenate anions was washed with an alkaline solution of sodium perchlorate (pH

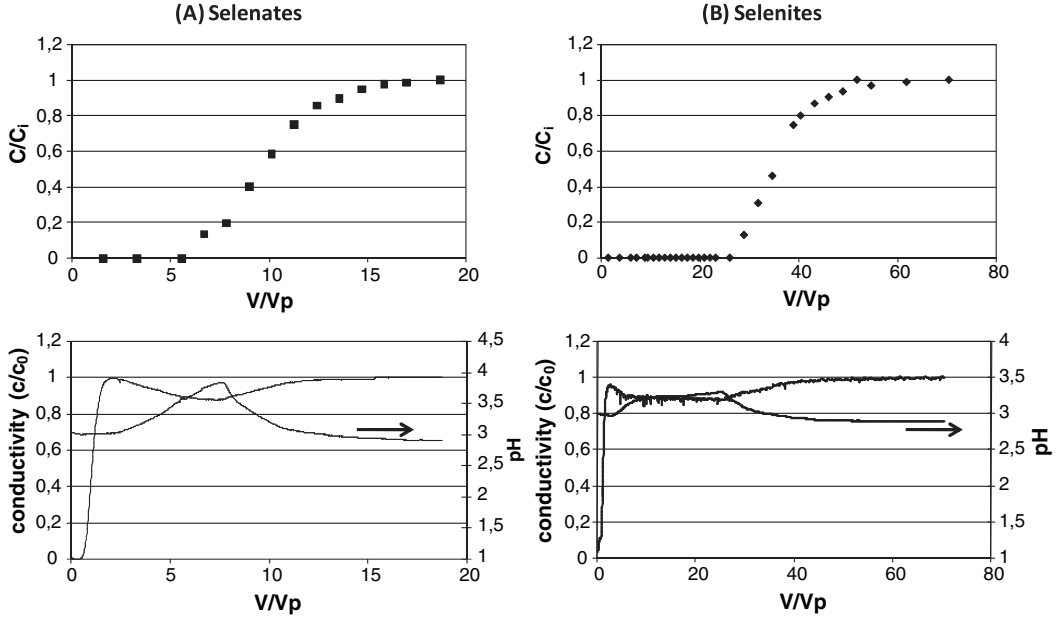

Fig. 7. (a) Selenate breakthrough curve (C_{in} 5×10^{-4} mol L^{-1}, pH 3, flow rate 0.2 mL min^{-1}) and pH and conductivity evolution during the experiment. (b) Same information for selenite species (C_{in} 10^{-3} mol L^{-1}, pH 3, flow rate 0.2 mL min^{-1}). V_p is the porous volume of the column, V is the inlet volume of solution injected in the column.

Table 2
Effect of selenium form on the retention capacity of the column.

Selenium form	SeO_4^{2-}		SeO_3^{2-}
Inlet concentration [mol L^{-1}]	0.0005	0.001	0.001
Flow rate [mL min^{-1}]	0.2	0.2	0.2
q_{total} [μmol]	16.2	21.7	113.0
q_{eq} [μmol g^{-1}]	2.1	2.8	14.8
Δ pH	0.9	–	0.4

11, [$NaClO_4$] = 0.1 mol L^{-1}). A significant desorption was observed. Whereas column saturation was reached after $15V/V_p$, $20V/V_p$ of washing solution were necessary to fully desorb the retained selenate anions. A complete desorption of selenate anions was achieved before the effluent pH reached pH 4, which again agreed with batch results and the sorption edge observed for selenate species in Fig. 3b. After this alkaline desorption, the column was regenerated by acid washing (pH 3, [$NaClO_4$] = 0.1 mol L^{-1}) and used in another sorption cycle.

To get further insight into the sorption mechanism and the stability of the surface complexes formed, an acidic solution of $NaClO_4$ (pH 3) was pumped into the system after the column was saturated by either selenite or selenate ions. The treatment of the corresponding desorption curves (not shown), allowed the measurement of the molar quantities of desorbed selenium species (Table 3). Using such acidic conditions, both selenium forms were desorbed. The amount of released selenites corresponds to 40% of the adsorbed amount, whereas in the case of selenates, 72 and 100% were desorbed, for the columns saturated using [SeO_4^{2-}] = 0.0005 mol L^{-1} and 0.001 mol L^{-1} respectively. Selenate anions were therefore more easily removed in acidic conditions, which was related to the higher pH variation observed upon selenate sorption (Fig. 7a) compared to the selenite case (Fig. 7b). Subsequent purging of the column with an alkaline solution led to a full desorption of sorbed selenium species (Table 3). This behaviour suggested the presence of two different surface complexes involving selenite anions with different thermodynamic or kinetic constants. According to such an interpretation, the first complex would require alkaline conditions to be fully removed from the surface. It is worth noting that selenite ions were not desorbed at the same pH values (Figure S5 of supporting material) as selenate ions. As shown in Figure S5b, the alkaline desorption of a selenite-saturated column previously submitted to acid desorption, started at pH 4, reached a maximum around pH ∼ 6–7 and ended at pH 10. This concurred again with batch results that revealed a slight affinity of selenite for the rutile surface at near-neutral pH (Fig. 3a).

The influence of ionic strength on breakthrough curves was investigated changing the inlet selenium concentration. Results are shown in Figure S6 of supporting information. In the case of selenite ions, the decrease in ionic strength appeared to have a marginal influence, the onset of the breakthrough being slightly delayed at the lower ionic strength. No clear influence was visible for selenate anions.

Table 3
Desorption under different experimental conditions (D_{ac} – acidic desorption, q_{des} – desorbed quantity, D_{al} – alkaline desorption).

Selenium form	SeO_4^{2-}		SeO_3^{2-}
Saturated at [mol L^{-1}]	0.0005	0.001	0.001
$D_{ac} - q_{des}$ [μmol]	11.6	21.7	44.6
Desorption%	72%	100%	40%
$D_{al} - q_{des}$ [μmol]	3.8	–	62.6
Desorption%	23%	–	55%
Total	95%	100%	95%

3.5. Discussion on the possible surface complexes formed by selenium oxo-anions at the rutile-water interface

The question of the inner-sphere or outer-sphere nature of the surface complexes formed at the mineral–solution interface is often analyzed through the influence of ionic strength on sorption features. In the present work, the adsorption of selenite anions at the rutile surface was not conclusively affected by an increase in ionic strength, especially in acidic media (Fig. 3a). In the case of selenate anions, in acidic condition, a slight decrease in adsorption may be observed for increasing ionic strength (Fig. 3b). According to classical interpretations, this may indicate the formation of inner-sphere complexes for selenite and of outer-sphere complexes for selenate. However, it is now recognised that the effect of ionic strength cannot be used as the sole indicator of the inner or outer-sphere nature of surface complexes. According to Su and Suarez [10], the presence or absence of an ionic strength effect on sorption only provides macroscopic information on the relative affinity and no molecular level structural information can be deduced with confidence from such a feature.

Still, in the case of selenate adsorption, as $HSeO_4^-$ appears to be the most retained species, a pure electrostatic interaction can certainly not explain the whole complexation process. Indeed, for pH ≤ 5.5, i.e. when the rutile surface is positively charged, pure electrostatic interactions would favour the adsorption of SeO_4^{2-} with two negative charges, and in the case of selenate adsorption no sorption edge effect would be observed at pH 3. This strongly suggests that at least a part of the surface complexes formed with selenate species are inner-sphere complexes. This interpretation is confirmed by column desorption experiments. Indeed, Table 3 reveals that acidic desorption does not remove all sorbed selenate anions after adsorption at a Se concentration of 5×10^{-4} mol L^{-1}. As shown in Table 3 and Figure S5 of the supporting material, alkaline conditions are needed to fully desorb all selenate ions, thus showing the existence of some inner-sphere complexes for selenate. In the case of selenite, the effect of alkaline desorption is more marked, which shows that inner-sphere mechanisms are more important for selenite compared to selenate. In the case of selenite adsorption, this inner-sphere complexation is further evidenced by EXAFS experiments, even if drying could have partly converted some outer-sphere complexes to inner-sphere ones. Taking into account all this information, the inner-sphere complexes of both anions can be tentatively assigned to the formation of a bidentate complex with terminal hydroxyl groups (Eqs. (3) and (4)). The partial charges of hydroxyl groups used in both equations were obtained from Ref. [55] where a CD-MUSIC calculation was applied.

$$2TiOH_2^{+0.566} + HSeO_3^- \rightarrow [(TiO)_2SeOH]^{+0.132} + 2H_2O \quad (3)$$

$$2TiOH_2^{+0.566} + SeO_4^{2-} + 2H^+ \rightarrow [(TiO)_2Se(OH)_2]^{+1.132} + 2H_2O \quad (4)$$

Eq. (4) is consistent with the pH change observed in Fig. 7a for selenate sorption. Eq. (3) does not involve any pH change, which somehow contradicts the slight pH change observed upon selenite sorption. However, considering the fact that much more selenite is adsorbed, the pH change observed can be considered as a minor effect. In order to confirm the existence of the proposed bidendate complexes, *ab initio* calculation should definitely be performed to optimize the energy and geometry of the surface complexes formed onto typical rutile crystallographic planes. Results of such calculations will be presented in future works. These calculations will also explore the role of the molecular structure of selenite and selenate anions on the formation of these surface complexes. The tetragonal structure of selenate may indeed change the thermodynamics of the sorption process if compared to selenite. It must finally be pointed out that the sorption process may involve other types of surface complexes, especially in the case of selenate anions.

Indeed, in that case, column acidic desorption experiments remove 72% of the surface species, which suggests the occurrence of outer sphere complexes. Further information on such complexes could be obtained from in situ EXAFS experiments.

4. Conclusion

The combination of batch and column sorption experiments and spectroscopic analyses has revealed that both selenite and selenate ions could form surface inner-sphere complexes on rutile TiO_2 powder in acidic conditions and using $NaClO_4$ as background electrolyte. A bidentate complex was proposed for both anions, in agreement with most of the results obtained in the present study. At least a part of the surface complexes that were formed also involve an outer-sphere mechanism, especially for selenate species. In situ spectroscopic studies will be further needed to investigate the formation of these more versatile surface complexes, which may be of importance to have a clear picture of the parameters that can influence the mobility of selenate ions in the environment.

Acknowledgements

This work has been supported by the French National Research Agency (ANR) through the MIDIS project, contract number ANR-05-BLAN-0245-03. Jacques Lambert is acknowledged for his technical support on Raman and XPS experiments. Dr Valérie Briois is acknowledged for scientific and technical assistance on the SAMBA beamline at the Soleil synchrotron. Dr Edward McRae is warmly acknowledged for his comments concerning the manuscript.

Appendix A. Supplementary data

Supplementary data associated with this article can be found, in the online version, at doi:10.1016/j.jhazmat.2011.02.090.

References

[1] S.J. Hamilton, Sci. Total Environ. 326 (2004) 1–31.
[2] D.S. Han, B. Batchelor, A. Abdel-Wahab, J. Hazard. Mater. 186 (2011) 451.
[3] D. Peak, U.K. Saha, P.M. Huang, Soil Sci. Soc. Am. J. 70 (2006) 192.
[4] M. Rovira, J. Gimenez, M. Martinez, X. Martinez-Llado, J. de Pablo, V. Marti, L. Duro, J. Hazard. Mater. 150 (2008) 279.
[5] R. Lopez de Arroyabe Loyo, S.I. Nikitenko, A.S. Scheinost, M. Simonoff, Environ. Sci. Technol. 42 (2008) 2451.
[6] J.G. Catalano, Z. Zhang, P. Fenter, M.J. Bedzyk, J. Colloid Interface Sci. 297 (2006) 665.
[7] M. Duc, G. Lefevre, M. Fedoroff, J. Colloid Interface Sci. 298 (2006) 556.
[8] M. Martinez, J. Gimenez, J. de Pablo, M. Rovira, L. Duro, Appl. Surf. Sci. 250 (2006) 3767.
[9] M. Duc, G. Lefevre, M. Fedoroff, J. Jeanjean, J.C. Rouchaud, F. Monteil-Rivera, J. Dumonceau, S. Milonjic, J. Environ. Radioact. 70 (2003) 61.
[10] C. Su, D.L. Suarez, Soil Sci. Soc. Am. J. 64 (2000) 101.
[11] A. Manceau, Geochim. Cosmochim. Acta 59 (1995) 3647.
[12] A. Manceau, L. Charlet, J. Colloid Interface Sci. 168 (1994) 87.
[13] G.E. Brown Jr., G.A. Parks, C.J. Chisholm-Brause, Chimia 43 (1989) 248.
[14] K.F. Hayes, A.L. Roe, G.E. Brown Jr., K.O. Hodgson, J.O. Leckie, G.A. Parks, Science 238 (1987) 783.
[15] T. Zuyi, C. Taiwei, D. Jinzhou, D. XiongXin, G. Yingjie, Appl. Geochem. 15 (2000) 133.
[16] H. Wijnja, C.P. Schulthess, J. Colloid Interface Sci. 229 (2000) 286.
[17] D. Peak, J. Colloid Interface Sci. 303 (2006) 337.
[18] C.P. Schulthess, Z. Hu, Soil Sci. Soc. Am. J. 65 (2001) 710.
[19] C. Papelis, Environ. Sci. Technol. 29 (1995) 1526.
[20] C. Papelis, G.E. Brown Jr., G.A. Parks, J.O. Leckie, Langmuir 11 (1995) 2041.
[21] S.M. Hasany, A.M. Shamsi, M.A. Rauf, Appl. Radiat. Isot. 48 (1997) 595.
[22] A.L. Foster, G.E. Brown Jr., G.E. Parks, Geochim. Cosmochim. Acta 67 (2003) 1937.
[23] A. Walcarius, J. Devoy, J. Bessiere, Langmuir 20 (2004) 6335.
[24] J. Devoy, A. Walcarius, J. Bessiere, Langmuir 18 (2002) 8472.
[25] L. Charlet, A.C. Scheinost, C. Tournassat, J.M. Greneche, A. Gehin, A. Fernandez-Martinez, S. Coudert, D. Tisserand, J. Brendle, Geochim. Cosmochim. Acta 71 (2007) 5731.
[26] N. Mace, C. Landesman, I. Pointeau, B. Grambow, E. Giffaut, Adv. Cem. Res. 19 (2007) 157.
[27] I. Baur, C.A. Johnson, Environ. Sci. Technol. 37 (2003) 3442.
[28] E.A. Johnson, M.J. Rudin, S.M. Steinberg, W.H. Johnson, Waste Manage. 20 (2000) 509.
[29] K.A. Boult, M.M. Cowper, T.G. Heath, H. Sato, T. Shibutani, M. Yui, J. Contam. Hydrol. 35 (1998) 141.
[30] R.N. Collins, N.D. Tran, E. Bakkaus, L. Avoscan, B. Gouget, Environ. Sci. Technol. 40 (2006) 7778.
[31] Y. Nakamaru, K. Tagami, S. Ushida, Chemosphere 58 (2005) 1347.
[32] N.J. Barrow, P. Cartes, M.L. Mora, Eur. J. Soil Sci. 56 (2005) 601.
[33] S. Sharmasarkar, G.F. Vance, Adv. Environ. Res. 7 (2002) 87.
[34] D. Wenming, W. Xiangke, D. Jinzhou, W. Dongqi, T. Zuyi, J. Radioanal. Nucl. Chem. 240 (1999) 715.
[35] Y. Tachi, T. Shibutani, H. Sato, M. Yui, J. Contam. Hydrol. 35 (1998) 77.
[36] C. Papelis, Adv. Environ. Res. 5 (2001) 151.
[37] A. Yllera de Llano, G. Bidoglio, A. Avogadro, P.N. Gibson, P. Rivas Romero, J. Contam. Hydrol. 21 (1996) 129.
[38] F. Monteil-Rivera, M. Fedoroff, J. Jeanjean, L. Minel, M.G. Barthes, J. Dumonceau, J. Colloid Interface Sci. 221 (2000) 291.
[39] J. Das, B. Sairam Patra, N. Baliarsingh, K.M. Parida, J. Colloid Interface Sci. 316 (2007) 216.
[40] E. Breynaert, C. Bruggeman, A. Maes, Environ. Sci. Technol. 42 (2008) 3595.
[41] P. Zhang, D.L. Sparks, Environ. Sci. Technol. 24 (1990) 1848.
[42] U. Diebold, Surf. Sci. Rep. 48 (2003) 53.
[43] J. Vandenborre, R. Drot, E. Simoni, Inorg. Chem. 46 (2007) 1291.
[44] A. Imanishi, T. Okamura, N. Ohashi, R. Nakamura, Y. Nakato, J. Am. Chem. Soc. 129 (2007) 11569.
[45] Z. Zhang, P. Fenter, L. Cheng, N.C. Sturchio, M.J. Bedzyk, M. Predota, A. Bandura, J.D. Kubicki, S.N. Lvov, P.T. Cummings, A.A. Chialvo, M.K. Ridley, P. Benezeth, L. Anovitz, D.A. Palmer, M.L. Machesky, D.J. Wesolowski, Langmuir 20 (2004) 4954.
[46] H. Perron, C. Domain, J. Roques, R. Drot, E. Simoni, H. Catalette, Theor. Chem. Acc. 117 (2007) 565.
[47] H. Perron, J. Vandenborre, C. Domain, R. Drot, J. Roques, E. Simoni, J.-J. Ehrhardt, H. Catalette, Surf. Sci. 601 (2007) 518.
[48] H. Perron, C. Domain, J. Roques, R. Drot, E. Simoni, H. Catalette, Radiochim. Acta 94 (2006) 601.
[49] H. Perron, C. Domain, J. Roques, R. Drot, E. Simoni, H. Catalette, Inorg. Chem. 45 (2006) 6568.
[50] L. Zhang, N. Liu, L. yang, Q. Lin, J. Hazard. Mater. 170 (2009) 1197–1203.
[51] K. Shi, X. Wang, Z. Guo, S. Wang, W. Wu, Colloid Surf. A: Physicochem. Eng. Aspects 349 (2009) 90–95.
[52] L. Svecova, S. Cremel, C. Sirguey, M.-O. Simonnot, M. Sardin, M. Dossot, F. Mercier-Bion, J. Colloid Interface Sci. 325 (2008) 363–370.
[53] I. Puigdomenech, Medusa: equilibrium diagrams using sophisticated algoritms, computer program, Royal Institute of Technology KHT, Stockholm, Sweden, http://www.telia.com/~u156651596, last update 18th February 2004.
[54] M.L. Machesky, M. Predota, D.J. Wesolowski, L. Vlcek, P. Cummings, J. Rosenqvist, M.K. Ridley, J.D. Kubicki, A. Bandura, N. Kumar, J. Sofo, Langmuir 24 (2008) 12331–12339.
[55] M.K. Ridley, T. Hiemstra, W.H. van Riemsdijk, M.L. Machesky, Geochim. Cosmochim. Acta 73 (2009) 1841–1856.